Dynamic Stresses in Weld Metal Hot Cracking

The dynamic relationship between mechanical and metallurgical factors influenced by restraint and welding parameters creates conditions favorable to hot cracking

BY T. ZACHARIA

ABSTRACT. This paper presents the results of a study aimed at understanding the influence of dynamic stresses, induced by thermal and mechanical loading, on weld metal hot cracking. The study attempts to resolve the relationship between the dynamic stress distribution in the specimen, particularly near the trailing edge of the pool, and the observed cracking behavior in a Sigmajig test specimen. The transient stress distribution in the specimen resulting from mechanical and thermal loading was calculated for a Type 316 stainless steel specimen. The initiation and propagation of the crack during welding was visually monitored using a stroboscopic vision system. The numerical results were used to understand the initiation and propagation of weld metal hot cracks during controlled welding of a specimen subjected to external restraint. The results of this study indicate that for hot cracking to occur, there exists a dynamic relationship between the metallurgical and mechanical factors, which can be influenced by the welding conditions and mechanical restraint.

Introduction

Hot cracking, which occurs during welding, is a major problem that affects the welding and weldability of a number of structural materials. Despite being one of the most investigated phenomena in welding (Refs. 1–16), hot cracking still remains a major problem for many advanced (Refs. 5–7) and conventional alloys (Refs. 8–16).

Hot cracking is believed to occur during the last stages of solidification, near a local solidus that could be significantly lower than the equilibrium solidus of the alloy. It generally occurs when the thermal and mechanical strains exceed the ductility of the almost solidified weldment. Three theories, shrinkage brittleness (Ref. 17), strain (Ref. 18), and supersolidus cracking (Ref. 19) are currently offered to explain hot cracking in alloys. The shrinkage-brittleness theory suggests that hot cracks develop during the mushy stage, if a critical level of strain is exceeded, when the coherent network of dendrites crack open to relieve the strain. The strain theory, on the other hand, suggests that hot cracking can occur only during the last stages of solidification, when continuous liquid films are distributed along the solidification grain boundaries. In the 1960s, Borland developed the generalized supersolidus cracking theory (Ref. 19), which includes concepts from both the previous theories. A good review of the theories mentioned above is available in References 1 and 2. While each of the above theories offer significant insights into hot cracking, each also has its limitations and can only be used as a guideline for interpreting experimental data.

It is clear from reviewing the hot cracking theories that for cracking to occur both metallurgical and mechanical factors must be present. It is well established that during welding, the nonuniform thermal distribution in and around the weldment generates stress and strain gradients. Although considerable work related to the metallurgical factors affecting hot cracking has been performed over the years (Refs. 1–21), very little has been done to understand the mechanical factors that affect hot cracking in welding. There have been some studies that attempted to study the thermal stresses and strains that occur during welding. However, there has been no attempt, until recently (Refs. 22, 23) to correlate the weld metal cracking response to the thermal-mechanical strains that develop in the weldment during welding.

This paper presents the results of a study aimed at understanding the mechanism of hot cracking in a specimen subjected to external restraint. A recently developed hot-cracking test, the Sigmajig test (Ref. 20), was used to study the cracking response, during welding, of a material under mechanical loading. The study

KEY WORDS

Weld Metal
Hot Cracking
Dynamic Stresses
Mechanical Loading
Thermal Stress
External Restraint
Type 316 SS
Sigmajig Specimen
Metallurgy
Mechanical Factors

T. ZACHARIA is leader of the Materials Process Modeling Group, Metals and Ceramics Division, Oak Ridge National Laboratory, Oak Ridge, Tenn.

Table 1 — Chemical Composition of 0.25-mm-Thick Type 316 Stainless Steel (Ref. 18)

	Composition (wt-%)
C	0.018
Mn	1.70
P	0.032
S	0.010
Si	0.34
Ni	12.16
Cr	17.04
Mo	1.98
Cu	0.05
N	0.047

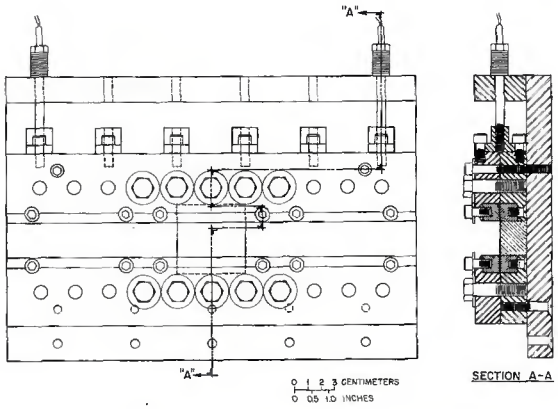

Fig. 1 — Schematic of the Sigmajig test fixture (Ref. 20).

attempts to resolve the relationship between the dynamic stress distribution in the specimen, particularly near the trailing edge of the pool, and the observed cracking behavior. The transient stress distribution in the specimen resulting from the pre-applied loading as well as thermal loading was calculated for a Type 316 stainless steel (SS) specimen. The initiation and propagation of the crack during welding was visually monitored using a stroboscopic vision system. The calculated transient stress state in the Sigmajig specimen was used to understand the initiation and propagation of hot cracks during welding under controlled conditions. Analyzing the Sigmajig test provided an opportunity not only to understand the test better, but also to understand the fundamental mechanisms, mechanical and metallurgical, that cause cracking during welding.

Procedures

Material

The material used in this investigation was a commercial Type 316 SS alloy, which is moderately sensitive to hot cracking. The chemical composition is listed in Table 1 (Ref. 20).

Sigmajig Testing

For most practical purposes, the crack susceptibility of a material is assessed by one of any number of hot cracking tests. Many laboratory and production line tests have been developed to evaluate the hot cracking susceptibility of structural materials (Refs. 3, 4). Recently, the Sigmajig test (Ref. 20) has been developed to quantitatively assess the crack susceptibility in thin sheet.

The Sigmajig test fixture is shown schematically in Fig. 1. The fixture applies a transverse stress, prior to welding, to a 50-mm-square (2-in.) specimen held firmly between steel grips. After preloading, an autogenous gas tungsten arc (GTA) weld is produced along the specimen centerline. The applied stress is sequentially increased, specimen by specimen, until centerline cracking initiates. The basis of the test is the determination of the threshold stress above which a centerline crack forms at the trailing edge of the weld pool (Ref. 20).

Sigmajig tests were performed on 0.25-mm-thick (1-in.) sheet material, which had a prior cold work of ~25% (Ref. 21). Full penetration autogenous GTA welds were made in the horizontal position with a Hobart Cyber-Tig II welding machine using a 1.6-mm (1/16-in.), 2% thoriated tungsten electrode. The welding parameters used in this investigation are: arc current 20 A DCEN and a travel speed of 14.8 mm/s (30 in./min). The welding current and duration are entered through digital switches, enabling accurate programming. The arc length was 0.76 mm (0.03 in.). Argon cover gas with a flow rate of 8 L/min (142 cm^3/s) was used.

Following Sigmajig testing, selected welds were mounted and polished for optical metallography. Samples were prepared using standard procedures and then etched using HNO_3 and H_2O.

Numerical Analysis

The stress distribution in the Sigmajig specimen was calculated using a coupled thermal-mechanical model. The details of the calculation and the computational models are documented elsewhere (Refs. 24–26). The temperature and stress distribution during Sigmajig testing was obtained by numerically solving the governing equations (Refs. 24–26) that represent the essential physical features of the process. In the solution of the dynamic stress distribution in the specimen, a plane strain assumption was utilized. This assumes that all the displacement occurs in the plane of calculation (the plane of the sheet) and that the displacement normal to this plane is zero. The material properties, such as yield strength, elastic and plastic moduli, coefficient of thermal expansion, Poisson's ratio, thermal conductivity, density, heat capacity, and viscosity, were all treated as temperature dependent in the calculation (Ref. 26).

Figure 2 shows the finite element mesh used for the two-dimensional, plain strain analysis. The finite element mesh consisted of 1500 elements, with the smaller elements near the weld centerline. Symmetry about the longitudinal axis was assumed in the calculation. In the stress analysis, a zero displacement boundary condition along the x-axis was used to represent restraint due to the fixture. The material behavior was represented by a temperature-dependent elasto-plastic model (Ref. 25). The result-

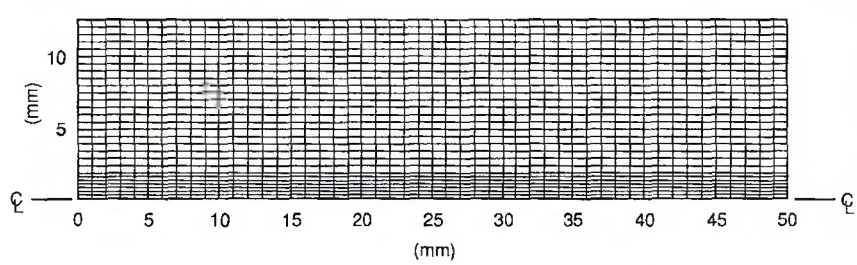

Fig. 2 — The grid system used for calculating the dynamic stress distribution during testing.

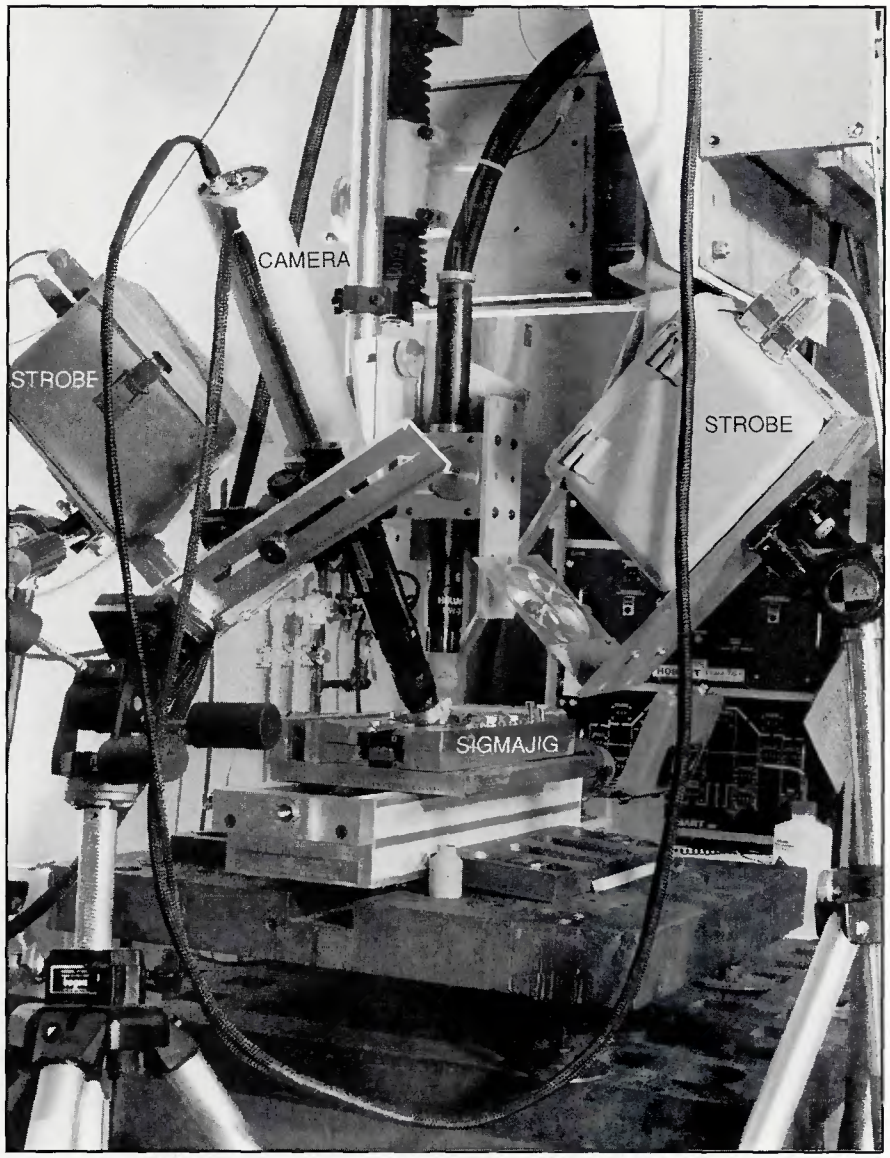

Fig. 3 —The stroboscopic vision system setup.

ing moving arc problem was solved for the entire length of the specimen.

Visual Examination

Crack initiation and growth in the Sigmajig specimen was observed using a stroboscopic weld vision system shown in Fig. 3. The camera system consists of two strobe illumination units, a camera head, and a system controller. A specialized video camera head provides electronic shuttering capability and sufficient optical sensitivity. The vision system uses an image intensifier tube used primarily for night vision. The tube can produce a 20,000-fold increase in the brightness of an image. A separate system controller sends appropriate trigger commands to fire the strobe units and to initiate shuttering.

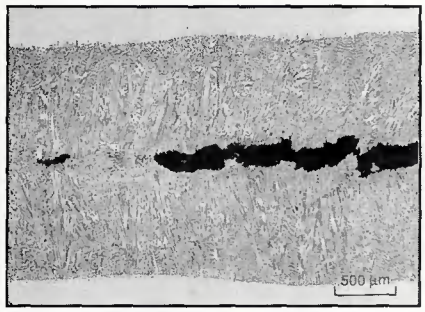

Fig. 4 — Optical photomicrograph of the Sigmajig specimen showing partial centerline cracking in the fusion zone.

Results

Sigmajig Testing

The cracking response of the Type 316 alloy given in Table 1 was established using the Sigmajig test. The threshold stress of this heat of Type 316 stainless steel was measured to be 124 MPa (18 ksi), at the lower end of the range, 103 to 344 MPa (15 to 50 ksi), for commercial heats. The applied stress was varied from 124 MPa (18 ksi) to 206 MPa (30 ksi) in order to change the stress distribution in the specimen and produce different levels of cracking. Figure 4 shows an optical micrograph of the weld fusion zone showing partial centerline cracking in the Sigmajig specimen. In the extreme case, the applied stress produced complete separation and failure of the specimen. Figure 5 shows a typical fracture surface of the test showing classical hot cracking or solidification cracking, characterized by the presence of a liquid film. Also, with increased applied stress, some amount of necking was observed near the centerline. This is in agreement with previous observations (Ref. 21).

Numerical Results

The sequence of events in Sigmajig testing involves preloading the specimen to a desired level, followed by autogenous GTA welding. Therefore, in the initial phase, the test is very similar to that of a tensile test. In the present analysis, the preloading was presumed to be done over a 2-s interval. Figure 6 shows the calculated stress distribution in the sheet specimen, prior to welding, for a pre-applied load of 2224 N (500 lb). The stress distribution in the specimen computed transverse to the welding direction (Fig. 6A) reveals stress concentration at the corners due to the restraint from the fixture. Overall, the calculations reveal a tensile stress field everywhere in the specimen. The maximum stress at the corners is close to 330 MPa (48 ksi), and the minimum stress level is close to 130 MPa (18 ksi). At the same time, transverse to the loading direction, the calculated results (Fig. 6B) show compressive regions near the two free edges, due to the Poisson effect. During tensile testing, it is this component of the stress that causes the material to neck down. These results are consistent with expected behavior during the preloading phase.

After preloading to the desired level, an autogenous bead-on-plate weld is made on the specimen to assess the hot cracking tendency of the weld metal under the imposed thermal and mechanical loading conditions. Figure 7 shows the calculated temperature distribution in the specimen after 4 s. The resulting stress distribution, computed transverse to the welding direction, for a pre-applied stress of 172 MPa (25 ksi) is presented in Fig. 8. Ahead of the weld pool, the result shows a compressive stress possibly due to the restraint by the cooler material further from the heat source.

Contrary to our expectations, the results also show a compressive stress behind the weld pool. Further behind the weld pool, the stresses along the weld centerline become tensile. If the material is unable to accommodate the tensile stresses with sufficient elastic or plastic deformation and if a susceptible solid plus liquid microstructure exists in the tensile region, then hot cracking may develop along the weld centerline at the weakest location in the specimen. Since the temperature distribution in the specimen changes as a function of time and location, it is expected that the resultant thermal stresses also will change.

The calculations were repeated for different levels of applied stress, maintaining the same welding parameters. Figure 9 shows the stress distribution, computed transverse to the welding direction for an applied stress of 103 MPa (15 ksi) and 172 MPa (25 ksi). For the sake of clarity, only the compressive envelope (0 MPa Contour) surrounding the weld pool is plotted. Four isotherms ranging from 1400 to 1700 K are overlaid on the plot. It is clear that the compressive envelope surrounding the weld pool changes as a function of the applied stress, shrinking with increasing mechanical restraint. As a result, with increased mechanical loading, the location behind the weld pool where the transverse stress field changes from compression to tension moves closer to the trailing edge and possibly to a more susceptible microstructure. It must be pointed out that the mechanical model that was solved may not be accurate at temperatures very close to the melting point of the material. However, it is expected that the general trends should be reasonably accurate.

As already mentioned, a compressive stress at the trailing edge was not expected and the inclination was to dismiss the results as an inability of the mechanical model to describe the trailing edge of the weld pool with sufficient accuracy.

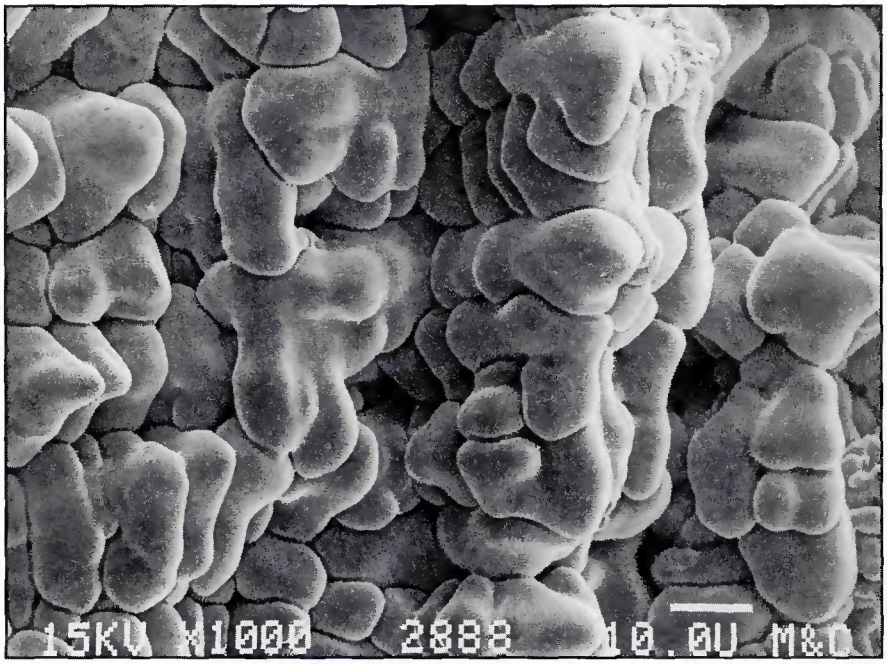

Fig. 5 — Typical crack surface of Sigmajig specimen showing classic hot cracking.

However, in reviewing the published literature on thermal stresses during welding, it became apparent that some experimental studies had reported the possibility of a compressive stress at the trailing edge of the weld pool (Refs. 27–29). Johnson (Ref. 27) studied dynamic plastic strains during GTA welding using Moire fringe analysis. He suggests that the material surrounding the weld pool must experience a compressive stress depending on the temperature distribution around the weld pool. As an example, he considered the two cases shown in Fig. 10. In the case of spot GTA welding, the hot metal surrounding the stationary heat source is restrained by the cooler metal further from the heat source. The restraint is uniform all around, thus the resulting stress pattern is uniform. With increasing heat input, the metal near the heat source will be compressed on all sides, and the hottest material near the solid-liquid interface begins to yield in compression.

For the case of a moving heat source, the presence of a compressive stress all around is not intuitively obvious. The temperature distribution is symmetrical about the welding direction. However, along the welding direction, the moving heat source produces a completely asymmetrical thermal distribution. As discussed above, for the case of spot GTA welding, thermal stress will be generated due to the nonuniform thermal distribution. However, for the moving heat source, the compressive stress would be much more intense in the front of the arc than behind it (Ref. 27). Johnson (Ref. 27) suggests that this asymmetry in the compressive stress field, in the welding direction, would cause the plastically deforming metal to shift rearward, so as to reduce the unbalanced front-to-rear stress pattern. The metal movement

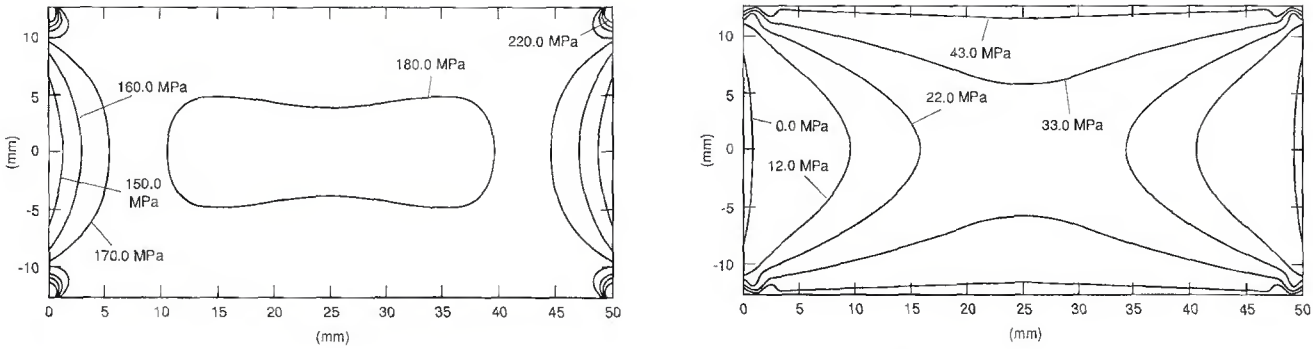

Fig. 6 — Calculated stress distribution in the Sigmajig specimen for a pre-applied load of 2224 N (500 lb). A — Transverse component of stress; B — longitudinal component of stress.

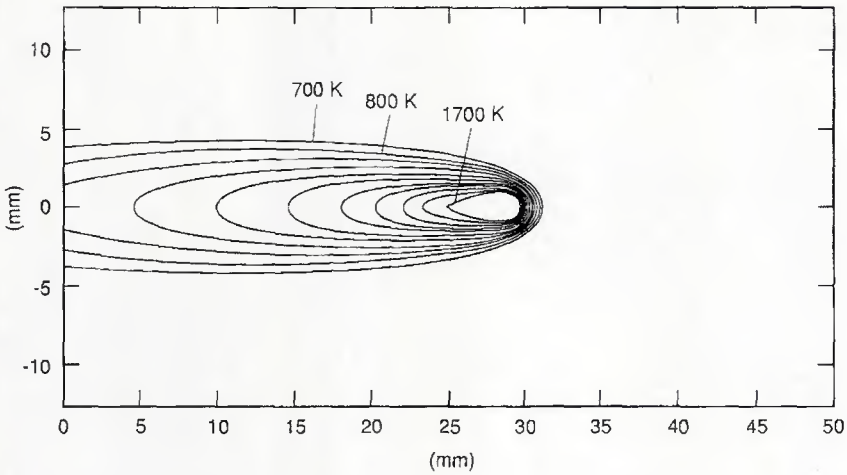

Fig. 7 — Calculated temperature distribution in the Sigmajig specimen after 4 s.

would clearly be dependent on the material properties and the temperature distribution near the weld pool. No attempt was made to quantitatively study this behavior.

In a separate work, Chihoski (Refs. 28, 29) attempted to resolve the stress field around a moving weld pool. His motivation was to address the disagreement between the accepted and apparently obvious view of a tensile stress at the trailing edge of the weld pool and a proposed compressive stress at the trailing edge of the weld pool. The work clearly showed, using Moire fringe analysis, that the thermal stress behind the weld pool was compressive largely due to the plastic flow of material from the front to back. The study showed that further behind the weld pool the stress changed from compressive to tensile. In addition, the results clearly showed that changing the welding conditions, such as welding speed or material or others, brought about changes in the extent and magnitude of the stress fields and the location of transition from a compressive field to a tensile field. The numerical results obtained in this study are in excellent qualitative agreement with the experimental results of Johnson (Ref. 27) and Chihoski (Refs. 28, 29).

Direct Observation of the Weld Area

Our current understanding of cracking mechanisms relies on careful deductions and speculations based on metallographic inspection, subsequent to welding, of the weld solidification structure and the crack morphology. An improved understanding of weld metal hot cracking can be obtained by direct visual observation of weld solidification and solidification cracking. Previous attempts at direct visual observation of weld solidification cracking have had very limited success (Ref. 30), primarily due to the lack of adequate resolution.

Welding represents an extremely difficult problem for in-situ observations, particularly due to the very high temperatures and the intense arc plasma. The molten weld pool and the solidification front are submerged within the luminous volume of the arc plasma. Viewing is further degraded due to the extreme variation in the brightness within the viewing area. For example, during arc welding, one can expect an intense bright area in the middle of the pool as opposed to the periphery of the weld pool. Consequently, direct viewing of the weld pool using conventional video techniques is difficult. Infrared cameras are commonly used to view the weld area during welding. The technique monitors longer infrared wavelengths emitting from the weldment to provide information on temperature. However, these images have limited spatial resolution and cannot provide precise information on finer details of the weld.

In the present investigation, a stroboscopic weld vision system was used to study weld solidification and cracking in a Sigmajig specimen. Figure 11 is a sequence of photographs showing different stages of crack initiation and growth during Sigmajig testing of Type 316 stainless steel. This series of pictures was obtained for an applied stress of 193 MPa (28 ksi), which is more than the threshold stress of 124 MPa (18 ksi) for this heat of material. The welding speed used is 14.8 mm/s (30 in./min), as noted earlier. Since the Sigmajig specimen is 50-mm (2-in.) long, the entire test takes 4 s to complete after arc initiation. The video technology used records 30 frames per second, each frame consisting of two fields. Therefore, up to 240 separate fields or pictures of the weld pool are recorded during the entire test duration. In order to provide a fixed frame of reference, the electrode and the camera head were held stationary, and the fixture and specimen were moved.

Initially, the arc interacts with the leading edge of the specimen and the molten metal beads up, due to surface tension, along the solid-liquid interface. With continued welding, the molten metal accumulates along the interface until sometime later when the weld pool is established. As a result, a weld pool, in the traditional sense, is not formed until later when the advancing solidification front envelopes the liquid at the trailing edge. Once formed, the weld pool responds to the overall heat transfer conditions, adjusting its shape to a tear drop, and follows the welding arc. Figure 11A shows a well-defined trailing edge of the molten weld pool. It is clear from the photograph that there is no obvious separation or centerline crack at the trailing edge of the weld pool. Figure 11B shows the first evidence of crack initiation and separation along the weld centerline. Notice that the location of the crack is clearly a significant distance behind the

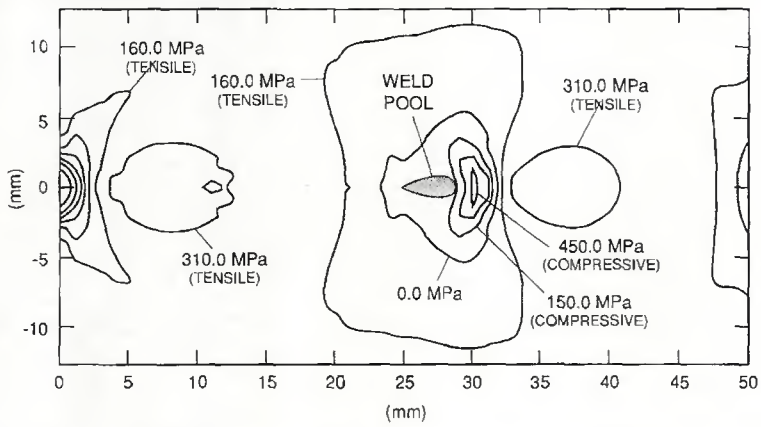

Fig. 8 — Calculated stress distribution in the Sigmajig specimen after 4 s.

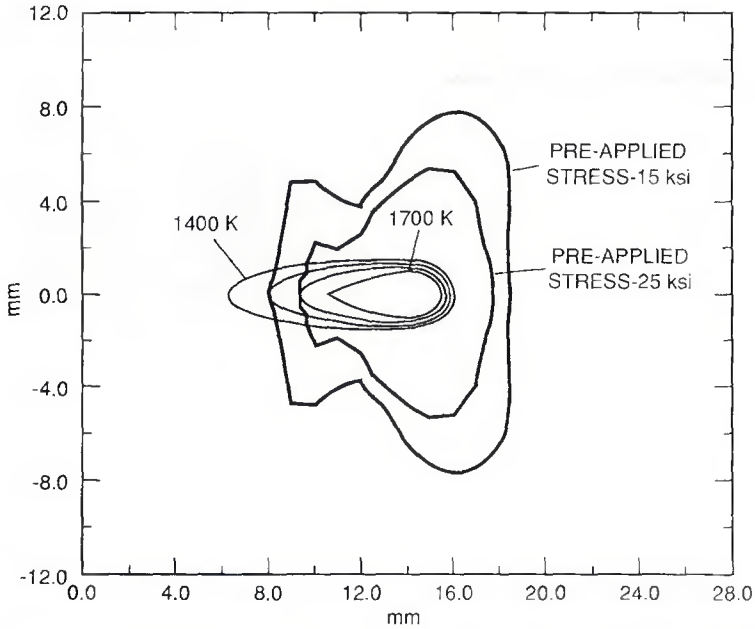

Fig. 9 — Compressive envelope surrounding the weld pool for two levels of mechanical loading.

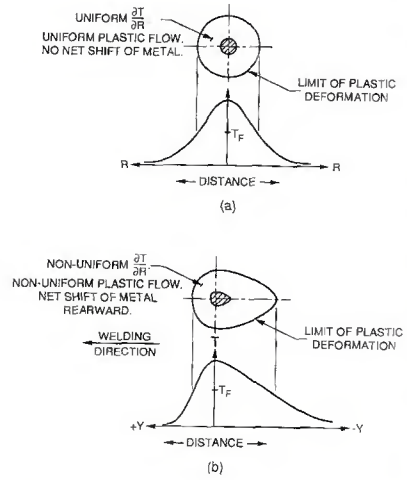

Fig. 10 — Comparison of thermal effects for a stationary and a moving heat source. The different temperature distributions give rise to different shapes and characteristics of the region where plastic flow takes place (Ref. 25).

trailing edge of the weld pool. When first observed, the location of the crack was surprising since it was expected that the crack would form at or very near the trailing edge of the weld pool. If the stress distribution in the specimen is favorable, this crack would grow as shown in Fig. 11C. With continued welding, the photograph shows the crack following the trailing edge of the weld pool. Since the applied load is fairly constant, as the crack grows, the applied stress increases due to decreased load-bearing area. As a result, the crack front (tip) advances toward the trailing edge of the weld pool as shown in Fig. 11D, ultimately producing complete failure of the specimen.

From the photographs, it is clear that the centerline crack initiates at a finite distance behind the weld pool. Once initiated, if the conditions are favorable, the crack grows toward the trailing edge and follows the weld pool. The fact that the crack initiates at a distance behind the weld pool became apparent when the Sigmajig test was repeated at a slightly lower applied stress of 172 MPa (25 ksi). Figure 12 shows a macrograph of the Sigmajig specimen after testing, showing a centerline crack extending from almost the midpoint to the terminal region of the weld. The crack surface was examined using a scanning electron microscope (SEM) to verify that it was hot cracking. Figure 13 shows an SEM photomicrograph of the fracture surface that is typical of hot cracking. Figure 14 shows the last two frames recorded during in-situ observation of the test. Surprisingly, the images did not show any cracks. It is clear from the photograph that there is no obvious separation or centerline crack within the field of view. Careful examination of the photographs revealed a slight depression along the centerline, where the terminal liquid appears to be stretched, which could be an indication of impending separation.

Discussion

In reviewing of the hot-cracking literature (Refs. 1–19), it became apparent that the overwhelming majority of these studies have concentrated on metallurgical aspects of cracking. Most of these studies have dealt with the essential mechanical factors in a very cursory manner, simply assuming a tensile stress field at the trailing edge of the weld pool where solidification is occurring. During welding, both tensile and compressive stresses are invariably present in a solidifying weldment due to nonuniform thermal distribution and other mechanical restraints. Since all alloys do not hot crack, it is clear that some liquid-plus-solid microstructures are more susceptible to hot cracking than others, stresses being equal. By the same token, not all welds in a given alloy hot crack, suggesting that a certain critical level of stress must be exceeded at some location in an alloy containing a susceptible mi-

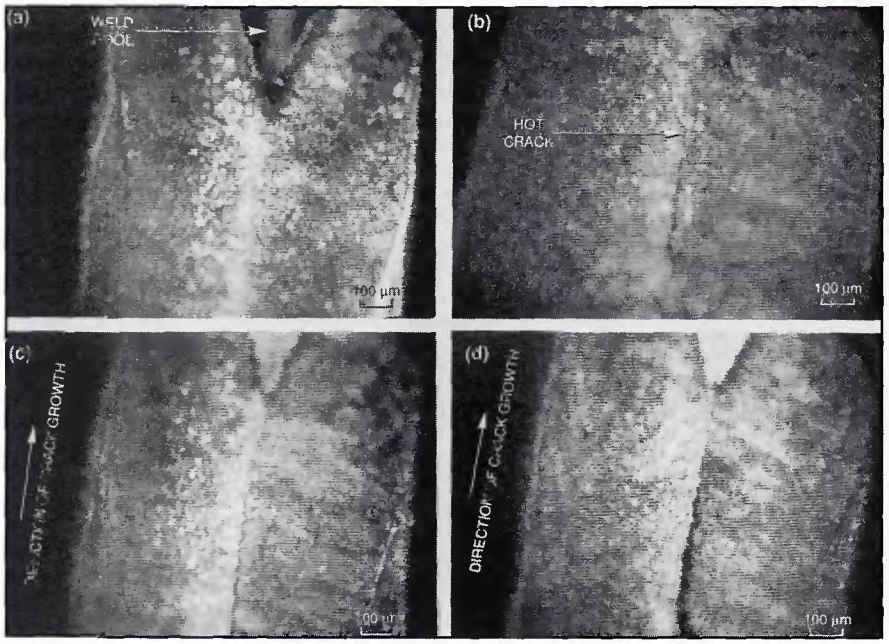

Fig. 11 — Sequence of photographs showing various stages in the Sigmajig testing.

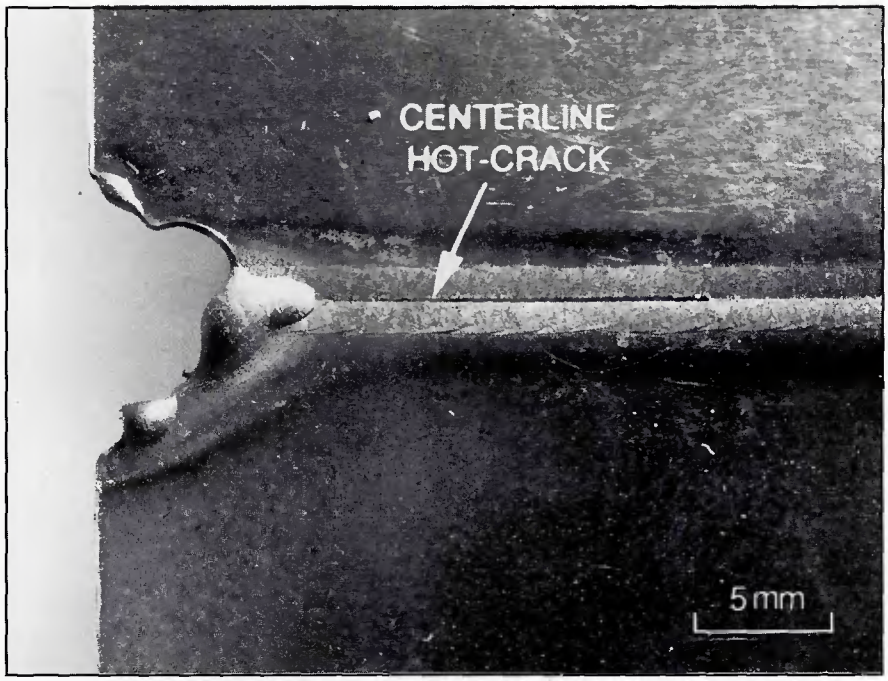

Fig. 12 — Macrograph of the Sigmajig specimen showing centerline crack.

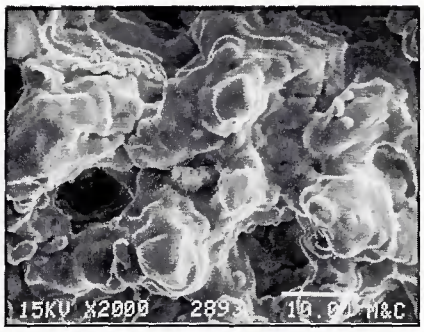

Fig. 13 — SEM photomicrograph of the fracture surface shown in Fig. 12 that is typical of hot cracks.

crostructure. Clearly, it would be desirable to understand the nature of this stress, the location where the crack initiates, whether it is at the trailing edge of the weld pool or some other location, and the stress state that promotes crack propagation.

In considering hot cracking in a weld between two parallel sheets of an aluminum alloy, Pumphery and Jennings (Ref. 17), using the model shown in Fig. 15, suggested that longitudinal cracking results when the total contraction comprised of contraction in zone BC (cooling region) minus the expansion in zones AB and CD (heating region) exceeds a critical value. Intuitively, it is easy to understand the argument that prior to solidification, the material goes through a phase change from solid to liquid, thereby completely relieving any stresses. Upon solidification, shrinkage strains develop at the trailing edge of the weld pool causing hot cracking or solidification cracking. While this explanation appears logical, any separation that occurs along the plane A-D is likely to heal because of the plentiful supply of liquid metal that is available from the molten pool. In order to form a hot crack, it is likely that the separation must be isolated from the reservoir of liquid metal (weld pool).

It is obvious that our understanding of the thermal strains and stresses that cause hot cracking in weldments is incomplete. In considering the mechanical factors that affect hot cracking, factors other than solidification shrinkage must be considered. Factors such as mechanical restraint, thermal distortion, and plastic deformation can alter the local stress distribution near the weld pool. Isolating the shrinkage stress and ignoring the other factors may be an oversimplification, and may not fully explain the relationship between dynamic stresses and hot cracking. It is necessary to understand the heat flow in the welded specimen and associated thermal stresses and distortion, when discussing hot cracking.

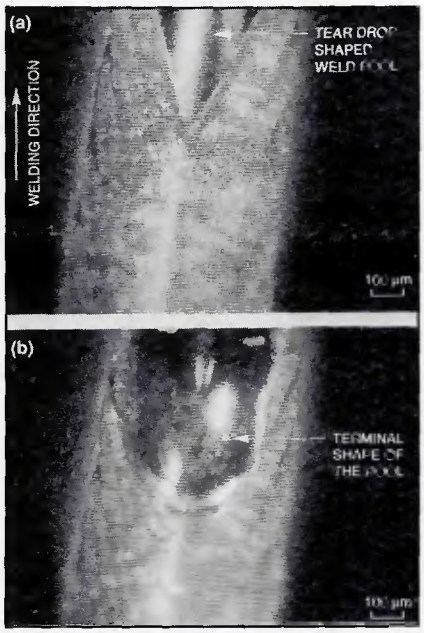

Fig. 14 — Photographs from in-situ observation of the Sigmajig test specimen shown in Fig. 12.

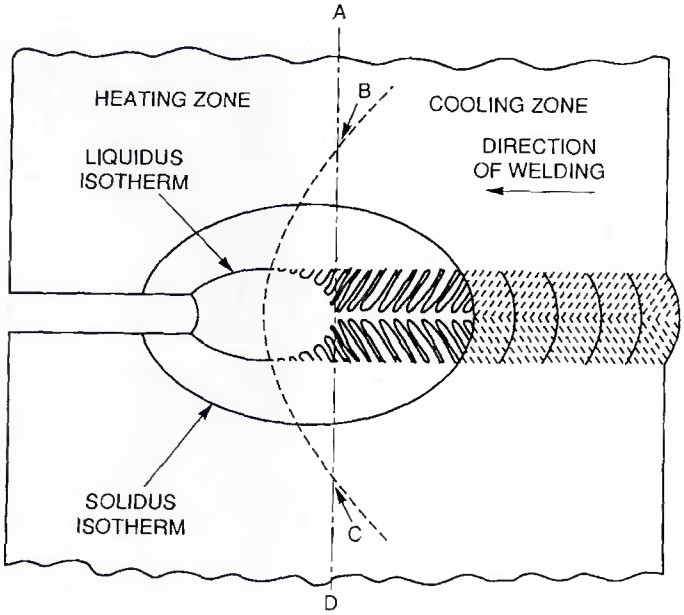

Fig. 15 — Conditions obtained in a butt joint weld between two parallel and restrained metal sheets (Ref. 19).

The results presented in Fig. 8 show a compressive envelope around the weld pool. Further behind the weld pool, the stress field acting transverse to the welding direction changes to a tensile field. Depending on the applied mechanical restraint experienced by the specimen during welding, this compressive envelope can be expanded or contracted around the weld pool.

The idea of a compressive stress at the trailing edge of the weld pool that changes to a tensile stress at some distance behind the pool is consistent with in-situ observations of crack initiation and growth. Figure 16 is a schematic showing the relationship of dynamic stresses to observed hot cracking behavior. Fig. 16A indicates the region of interest showing a liquid film extending from the trailing edge of the weld pool. The transverse stress acting on the weld centerline is presented schematically in Fig. 16C. The compressive stress immediately behind the pool prevents the formation of hot cracks at the trailing edge of the weld pool. At a discrete distance behind the weld pool, the transverse stress changes from compressive to tensile. If liquid is present, as shown in Fig. 16A, it is likely that hot cracks will form. If, on the other hand, due to changes in the composition of minor elements, the location of the terminal solidification temperature T_E is shifted as shown in Fig. 16B, it is unlikely that hot cracking would occur. Similarly, changes in the thermal distribution (welding speed, heat input, etc.) and external restraint can also shift the transition location (from compressive to tensile stresses), influencing the hot cracking behavior.

The Type 316 alloy used in this investigation is expected to solidify in the primary austenite mode (Ref. 21). During solidification as primary austenite, chromium, silicon, sulfur, and phosphorus are rejected to the liquid. Therefore, the last liquid that solidifies along the solidification grain boundaries may have relatively high concentrations of these elements. Matsuda, *et al.* (Ref. 3), observed particularly high levels of phosphorus along cell boundaries in fully austenitic weldments and related this to greater susceptibility of hot cracking in these alloys. Kujanpaa, *et. al.* (Ref. 14), has shown that the sulfur content in the liquid film, based on auger electron spectroscopy (AES) measurements of the crack surface, can be as high as 2000 times the bulk sulfur content. In the present alloy, containing 0.01 wt-% S, the sulfur content in the interdendritic liquid can be as high as 20 wt-%. This would imply, based on the binary Fe-S system, a solidification temperature of 1300°C (2372°F) for the terminal phase. At the extreme, continuous liquid films can be expected at temperatures as low as a 1000°C (1832°F) [Fe-S (938°C), Fe-P (1048°C], which is approximately 400°C (752°F) below the bulk solidus temperature of the alloy.

The threshold stress for this alloy was determined to be 124 MPa (18 ksi). Therefore, centerline hot cracks are not expected to form below an applied stress of 124 MPa (18 ksi). From Fig. 6A, for an applied stress of 103 MPa (15 ksi), the location where the stress changes from compressive to tensile is at a temperature of about 1500 K (1227°C). Increasing the applied stress to 172 MPa (25 ksi) shifts this point to a location that is at 1600 K (1327°C). Qualitatively, this agrees with the idea that centerline hot cracking initiates at a location well away from the weld pool, at or near the location where the temperature is close to a local solidus, which is lower than the equilibrium solidus of the alloy.

From the results of this study, it is clear that the dynamic stress distribution in a specimen during welding is very complex. As would be expected, the results also indicate that this stress field is sensitive to external restraint.

Summary and Conclusions

A study was conducted to understand the mechanism of hot cracking in a Type 316 austenitic stainless steel specimen subjected to external restraint. The emphasis of this study was to understand the dynamics of cracking due to mechanical and thermal loading in a material in which the cracking response is reasonably well understood metallurgically. State-of-the-art techniques were used to visually observe the hot cracks as they developed. Additionally, the dynamic stress state in the specimen was calculated for the welding conditions based on a knowledge of thermal and mechanical loading and material properties. Combining the different sources of information, an attempt was made to provide a better understanding of weld metal hot cracking.

The results clarified that centerline cracking in a full-penetration weld subjected to external restraint initiates at a location separated from the molten pool. This is contrary to the popular belief that cracking initiates at the trailing edge of the weld pool. Once initiated, the crack propagates and follows the trailing edge of the weld pool if the dynamic stress state and the metallurgical factors are favorable.

The numerical results indicate the presence of a compressive stress behind the weld pool that would prevent separation of the weld at the trailing edge of the weld pool.

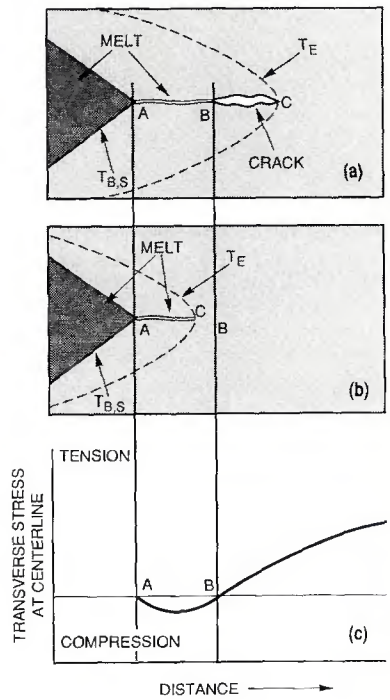

Fig. 16 — Conditions in a Sigmajig specimen, where an autogenous bead is deposited on a sheet subjected to external restraint.

The results reaffirmed that weld metal hot cracking that occurs during and immediately after welding is due to the presence of small quantities of liquid residing at solidification boundaries and, at the same time, being subjected to tensile strains.

The results of this study indicate that for hot cracking to occur, there is a necessary dynamic relationship between the metallurgical and mechanical factors, which can be influenced by the welding conditions and mechanical restraint.

Acknowledgment

The author thanks G. M. Goodwin, B. Radhakrishnan and S. Viswanathan for reviewing the manuscript and K. Spence for technical editing. The contributions of G. A. Aramayo, G. M. Goodwin, J. F. King and M. L. Santella are gratefully acknowledged. The Y-12 Development Division provided the financial support, and T. M. Mustaleski and M. Richey deserve special thanks for their support and encouragement. The research was sponsored by the U. S. Department of Energy, Assistant Secretary for Energy Efficiency and Renewable Energy, Office of Industrial Technologies, Advanced Industrial Materials Program, under contract DE-AC05-84OR21400 with Martin Marietta Energy Systems, Inc.

References

1. Savage, W. F., Nippes, E. F., and Good-

win, G. M. 1977. Effect of minor elements on hot-cracking tendencies of Inconel 600. *Welding Journal* 56(8): 245-s to 253-s.

2. Matsuda, F. 1989. Solidification crack susceptibility of weld metal. *Proceedings of the 2nd International Conference on Trends in Welding Research*, Gatlinburg, Tenn.

3. Goodwin, G. M. 1990. Hot cracking: measurement, mechanisms and modeling. *Welding Journal* 69(2): 26–31.

4. Goodwin, G. M. 1990. Test methods for evaluating hot cracking: review and perspective. *Proceedings of the First United States-Japan Symposium on Advances in Welding Metallurgy*, June 7-8, San Francisco, Calif., and June 12-13, Yokohama, Japan, pp. 37–49.

5. David, S. A., Jemian, W. A., Liu, C. T., and Horton, J. A. 1985. Welding and weldability of nickel-iron aluminides. *Welding Journal* 64(1): 22-s to 28-s.

6. David, S. A., Horton, J. A., McKamey, C. G., Zacharia, T., and Reed, R. W. 1989. Welding of iron aluminides. *Welding Journal* 68(9): 372-s to 381-s.

7. Santella, M. L., David, S. A., and White, C. L. 1985. Weldability of Ni_3Al-type aluminide alloys. *Mat. Res. Soc. Symp. Proc.* Vol. 39: 495–503.

8. Hull, F. C. 1967. Effect of delta ferrite on the hot-cracking of stainless steel. *Welding Journal* 46(9):399-s to 409-s.

9. Arata, Y., Matsuda, F., and Katayama, S. 1976. Solidification crack susceptibility in weld metals in fully austenitic stainless steel (report)-fundamental investigation on solidification behavior of fully austenitic and duplex microstructures and effect of ferrite on microsegregation. *Transactions of the Japanese Welding Research Institute* 5(2):35–51.

10. Brooks, J. A., and Lambert, F. J. 1978. The effects of phosphorus, sulfur and ferrite content on weld cracking of type 309 stainless steel. *Welding Journal* 57(5): 139-s to 143-s.

11. David, S. A., Goodwin, G. M., and Braski, D. N. 1979. Solidification behavior of austenitic stainless steel filler metals. *Welding Journal* 58(11): 330-s to 336-s.

12. Kujanpaa, V. P., David, S. A., and White, C. L. 1986. Formation of hot cracks in austenitic stainless steel welds — solidification cracking. *Welding Journal* 65(8): 203-s to 212-s.

13. Cieslak, M. J., Ritter, A. M., and Savage, W. F. 1982. Solidification cracking and analytical electron microscopy of austenitic stainless steel weld metals. *Welding Journal* (61)1: 1-s to 8-s.

14. Lippold, J. C., and Savage, W. F. 1982. Solidification of austenitic stainless steel weldments: part III — the effect of solidification behavior on hot cracking susceptibility. *Welding Journal* 61(12): 388-s to 396-s.

15. Cross, C. E., and Edwards, G. R. 1989. Welding of aluminum alloys, *Treatise on Materials Science and Technology*, Vol. 31d: 171–187.

16. Holt, M., Olson, D. L., and Cross, C. E. 1992. Interfacial tension driven flow model for hot cracking. *Scripta Met.* 26: 1119–1124.

17. Pumphrey, W. I., and Jennings, P. H. 1948. *J. Inst. Met.*, Vol. 75: 235–256.

18. Bishop, H. F., and Pellini, W. S. 1951. *A. F. S. Trans.* 1951.

19. Borland, J. C., and Younger, R. N. 1960. Some aspects of cracking in austenitic steels. *British Welding Journal* 71(1): 22–60

20. Goodwin, G. M. 1987. Development of a new hot-cracking test — Sigmajig. *Welding Journal* 66(1): 33-s to 38-s.

21. Goodwin, G. M. 1988. The effect of heat input and weld process on hot cracking in stainless steel. *Welding Journal* 67(4): 88-s to 94-s.

22. Brooks, J. A., Dike, J. J., and Krafcik, J. S. 1994. On modeling weld solidification cracking. To be published in the proceedings of the International Conference on Modeling and Control of Joining Processes, December 8-10, 1993, Orlando, Fla.

23. Zhilli, F., and Tsai, C. L. 1994. Modeling thermomechanical conditions of weld pool. To be published in the proceedings of the International Conference on Modeling and Control of Joining Processes, December 8-10, 1993, Orlando, Fla.

24. Zacharia, T., Eraslan, A., Aidun, D. K., and David, S. A. 1989. Three dimensional transient model for arc welding process, *Metall. Trans. B.* Vol. 20B: 645 to 659.

25. Hallquist, J. O. 1990. A vectorized implicit finite deformation finite element code for analyzing the static and dynamic response of 2-D solids with interactive rezoning and graphics, LSTC report 1006, Livermore Software Technology Corp., Livermore, Calif.

26. Zhu, Y. Y., and Zacharia, T. 1994. Three dimensional finite element analysis for welding processes. Submitted to the *AIAA Journal*.

27. Johnson, L. 1973. Formation of plastic strains during welding of aluminum alloys. *Welding Journal* 52(7): 298-s to 305-s.

28. Chihoski, R. A. 1972. Understanding weld cracking in aluminum sheet. *Welding Journal* 51(1): 24 to 30.

29. Chihoski, R. A. 1972. The character of stress fields around a weld arc moving on aluminum sheet. *Welding Journal* 51(1): 9-s to 18-s.

30. Matsuda, F., Nakagawa, H., Honda, Y., and Sorada, K. 1982. Direct observation of solidification and solidification cracking during GTA welding. *Proceedings of the Symposium of the Japan Welding Society*, November, 1982, Osaka, Japan, pp. 389–394.

RECOMMENDATIONS TO ASME FOR CODE GUIDELINES AND CRITERIA FOR CONTINUED OPERATION OF EQUIPMENT

The results contained in this bulletin were obtained through projects undertaken by the PVRC Task Group on Continued Operation of Equipment.

The objective was to make recommendations to ASME Codes and Standards to develop guidelines and criteria for continued operation of equipment. In addition, the task group had the responsibility of making recommendations for developing guidelines for evaluating piping, nondestructive examination of material degradation, and operation and maintenance history and life cycle management.

The price of WRC ***Bulletin 380 (April 1993)*** is $55.00 per copy, plus $5.00 for U.S. and Canada, or $10.00 for overseas, postage and handling. Orders should be sent with payment to the Welding Research Council, Inc. • 345 E. 47th St. • Room 1301 • New York, NY 10017 • (212) 705-7956.